
Article:
McKenna, Keith P. orcid.org/0000-0003-0975-3626 (2018) Structure, electronic properties, and oxygen incorporation/diffusion characteristics of the Σ 5 TiN(310)[001] tilt grain boundary. Journal of Applied Physics. p. 75301. ISSN 0021-8979

https://doi.org/10.1063/1.5016626

Structure, electronic properties, and oxygen incorporation/diffusion characteristics of the $\Sigma 5$ TiN(310)[001] tilt grain boundary

Keith P. McKenna

Citation: Journal of Applied Physics **123**, 075301 (2018);
View online: https://doi.org/10.1063/1.5016626
View Table of Contents: http://aip.scitation.org/toc/jap/123/7
Published by the American Institute of Physics

Structure, electronic properties, and oxygen incorporation/diffusion characteristics of the Σ5 TiN(310)[001] tilt grain boundary

Keith P. McKenna[a)]
Department of Physics, University of York, Heslington, York YO10 5DD, United Kingdom

(Received 21 November 2017; accepted 14 January 2018; published online 15 February 2018)

First principles calculations are employed to investigate the structure, electronic properties, and oxygen incorporation/diffusion characteristics of the Σ5 TiN(310) tilt grain boundary with relevance to applications of polycrystalline TiN in microelectronics and protective coatings. We show that the grain boundary does not significantly modify electronic states near the Fermi energy but does induce an upward shift of up to 0.6 eV in a number of deeper occupied bands. We also show that oxygen is preferentially incorporated into the TiN grain boundary (GB) but must overcome relatively high activation energies for further diffusion. These predictions are consistent with the "stuffed barrier model" proposed to explain the good barrier characteristics of TiN. We also show that while the oxidizing power of TiN GBs is not sufficient to reduce HfO_2 (a prototypical gate dielectric material), they can act as a scavenger for interstitial oxygen. Altogether, these results provide the much needed atomistic insights into the properties of a model GB in TiN and suggest a number of directions for future investigation. https://doi.org/10.1063/1.5016626

I. INTRODUCTION

Titanium nitride (TiN) finds applications as a gate electrode in advanced metal oxide semiconductor field effect transistors (MOSFETs),[1] electrodes for non-volatile resistive switching memory (ReRAM),[2–5] and as a diffusion barrier in a wide range of microelectronic devices.[6] In all of these applications, TiN is usually polycrystalline but relatively little is known about the properties of the associated grain boundaries (GBs). There is evidence from transport measurements and spectroscopic ellipsometry that GBs limit the electron mean free path in polycrystalline TiN and also modify its optical response.[7,8] GBs in TiN have also been suggested as preferred locations for the incorporation and diffusion of oxygen.[9–11] In devices, the incorporation of oxygen into TiN from an adjacent metal oxide phase (e.g., HfO_2 in a MOSFET) would create oxygen vacancy defects in the oxide that may contribute to undesirable effects such as leakage current and bias temperature instability.[12–14] Exchange of oxygen at a TiN/HfO_2 interface may also be an important factor for the functionality and stability of ReRAM devices.[3,15,16] However, despite much speculation, there is little direct information on the structure and properties of GBs in TiN. In particular, a number of important questions remain unanswered: how do GBs modify the electronic structure of TiN?, how readily does oxygen incorporate into TiN GBs compared to the bulk crystal and what chemical state does it adopt?, what are the thermodynamics of oxygen incorporation with respect to an adjacent oxide phase (HfO_2 being a particularly important example)?, and if oxygen is absorbed by GBs, how mobile is it and what is the mechanism for diffusion? Answering these questions is important for the technological applications in microelectronics discussed above and also for wider applications of TiN as protective and non-toxic coatings for metal components and biomedical implants.[17]

In this article, we perform first principles theoretical calculations to predict the structure, electronic properties, and oxygen incorporation and diffusion characteristics of a TiN GB. In particular, we consider the Σ5 TiN(310)[001] tilt GB as a model system that exhibits many characteristics of more general GBs—namely uncoordinated atoms, strained bonds, and excess volume. We identify two inequivalent GB structures which have very similar stability, suggesting both may coexist in real materials. While the atomic structures of the GBs are different, the corresponding properties are found to be quite similar. In particular, we find that there is very little perturbation of the electronic structure at the Fermi energy. However, deeper occupied electron states (in particular, Ti 3*p* and N 2*s* bands) are shifted to higher energies at GBs by up to 0.6 eV correlated with local variations in the electrostatic potential. O_2 incorporates into open regions at the GB gaining up to 3.1 eV per oxygen atom with respect to the gas phase. O_2 is predicted to dissociate into separated oxygen ions which acquire a charge of $-1.1e$ and form bonds with undercoordinated Ti atoms at the GB. We predict that TiN GBs are not able to extract lattice oxygen ions from an adjacent HfO_2 phase but do act as a scavenger for interstitial oxygen. The barrier to diffusion of oxygen along the GB is at least 1.7 eV suggesting TiN should represent a very benign electrode for MOSFET applications. However, in ReRAM applications, the non-equilibrium process driven by the applied electrical bias and Joule heating could conceivably lead to oxygen transfer.[3,15,16] These predictions are amenable to testing by a range of structural and spectroscopic probes—including scanning transmission electron microscopy, X-ray

a)Electronic mail: keith.mckenna@york.ac.uk

photoelectron spectroscopy[18] or electron energy loss spectroscopy—and provide much needed atomistic insights into the structure and electronic properties of GBs in TiN relevant to applications in microelectronics, photovoltaics, and optoelectronics.

The rest of this article in organized in the following way. In Sec. II, previous experimental and theoretical work on TiN and associated GBs is discussed. In Sec. III, we detail the first principles methods we employ to model the Σ5 TiN(310)[001] tilt GB. In Sec. IV, we present our predictions on its structure, electronic properties, as well as oxygen incorporation and diffusion. In Sec. V, we discuss links to the experiment and the factors that influence the accuracy and transferability of the results before summarizing our conclusions in Sec. VI.

II. BACKGROUND

Titanium nitride (TiN) is an inert and extremely tough ceramic material with applications as a protective layer for high strength metal components and a non-toxic coating for biomedical implants.[17] TiN adopts a rocksalt crystal structure with $a = 4.238$ Å.[19] Unusually for a ceramic material, TiN is also metallic (with electrical resistivity of ∼30–70 $\mu\Omega$ cm) and finds a number of applications which utilize this property. These include electrodes in advanced field effect transistors and emerging resistive switching memory technologies,[2–5,15] cathodes for high energy density lithium-sulfur batteries,[20] electrodes in photovoltaic cells, and materials for plasmonics.[21] Although a wide range of tilt and twist GBs can observed experimentally in TiN, tilt GBs on the [001] axis are very common in highly textured films.[22] A recent study on MgO (a material which has the same crystal structure as TiN) demonstrated the predominance of high site coincidence (low sigma) tilt GBs in such granular films.[23]

Investigations of electron transport and optical properties of TiN films grown under different conditions identified GBs as a source of increased scattering in nominally stoichiometric films.[7] A more recent study identified a significant discrepancy between the electrical resistivity determined optically and by transport measurements (with the latter being much higher) for thin TiN films.[8] This was attributed to increased electron scattering at GBs. However, direct information on the local electronic properties of GBs remains limited.

GBs in TiN are also believed to be favorable locations for the incorporation and diffusion of atoms from adjacent phases during growth and processing (e.g., oxygen, rare gas or metal atoms[11,24,25]) For example, studies of TiN oxidation kinetics suggest that oxygen is preferentially absorbed into GBs before surface oxidation begins.[9,11] The "stuffed barrier model" of Mändl *et al.* proposes that TiN retains good diffusion barrier properties even in the polycrystalline form as the otherwise fast diffusion paths that GBs would present are blocked by the incorporation of relatively immobile oxygen.[10] A related study showed that temperatures of the order of 560 °C are required before Al diffusion though an air exposed polycrystalline TiN film is appreciable.[24]

While first principles theoretical calculations have helped elucidate the properties of bulk TiN together with low index surfaces and point defects,[26] theoretical studies of GBs are relatively limited. Stable dislocation core structures in TiN and the associated Peierls stress have been studied using first principles methods.[27] A very recent study investigated the diffusion of Cu along the Σ5 TiN(210)[001] GB.[28] However, as far as we aware, there have been no theoretical studies of the electronic properties of GBs in TiN or their interaction with oxygen.

III. METHODS

Spin polarized density functional theory calculations using the projector augmented wave method are performed using the Vienna *ab initio* simulation package (VASP).[29–32] The following electrons are treated as valence: Ti (3*p*, 3*d*, and 4*s*), Hf (5*p*, 5*d*, and 6*s*), N, and O (2*s* and 2*p*) and expanded in a plane wave basis set (500 eV cut-off). The Perdew-Burke-Ernzerhof (PBE) functional is used to approximate exchange and correlation.[33] For the primitive unit cells, a $10 \times 10 \times 10$ Monkhorst-Pack *k*-point sampling scheme is used and the structures are fully optimized to a force tolerance of 0.01 eV/Å. The predicted bulk lattice constants of *m*-HfO_2 ($a = 5.145$ Å, $b = 5.192$ Å, $c = 5.329$ Å, and $\beta = 99.73°$) and TiN ($a = 4.252$ Å) are within 0.7% of the experiment and the electronic structure is also consistent with previous studies.[26,34] The calculated formation energies of bulk *m*-HfO_2 (−10.72 eV) and TiN (−3.46 eV) with respect to the bulk metal phases and molecular O_2 and N_2 are also consistent with the experiment [−11.58 eV (Ref. 35) and −3.50 eV (Ref. 36) per formula unit].

To model the GBs, we employ methods similar to those previously described in applications to a range of materials including silicon, MgO, HfO_2, and TiO_2.[37–42] In particular, we construct supercells that contain two mirror symmetric grains oriented such that the [310] direction is perpendicular to the GB plane. For GB supercells, *k*-point sampling is reduced to $5 \times 1 \times 1$. The structure of the supercell is optimized with respect to the position of all ions in the supercell, the translation of one grain against the other parallel to the GB plane and the length of the supercell perpendicular to the GB. We perform calculations using different grain thicknesses until the structure and GB formation energy is converged (results presented in the following use a grain thickness of at least 13 Å).

To model oxygen defects in the bulk crystals (neutral vacancies and interstitials), we construct supercells to minimize interactions between periodically repeated images. $3 \times 3 \times 3$ supercells of TiN and *m*-HfO_2 are employed (containing 216 and 324 atoms, respectively) ensuring a minimum separation between periodically repeated defects of 12.7 Å. For bulk supercells, only the gamma point in the Brillouin zone is sampled. For modeling incorporation and diffusion of oxygen in the GBs, supercells are doubled in the [001] direction to minimize artificial periodic interactions. For all defect calculations, full relaxation of the geometry is performed under a constant cell volume as appropriate for the dilute defect limit. We employ the Bader approach for analysis of the charge density as described in Ref. 43.

Barriers to diffusion are calculated using the climbing image nudged elastic band (NEB) method with 5 images along the diffusion path and forces are optimized to a tolerance of 0.01 eV/Å.[44]

IV. RESULTS

A. Grain boundary structure

Through a systematic search of possible rigid body translations of one crystal with respect to the other, we have identified two inequivalent stable structures for the Σ5 TiN(310)[001] GB. These structures are hereafter referred to as GB a and GB b (Fig. 1). Viewed in the [001] direction, both GBs are symmetric about the GB plane and consist of a periodic array of structural units. The main difference between the two structures is that the structural units are more open in GB a than in GB b. The additional "open space" associated with a GB can be conveniently quantified by the excess volume (defined as the excess volume per unit area of GB relative to that of the bulk crystal—therefore having the unit of length).[42] The excess volume of GB a (1.3 Å) is larger than that of GB b (0.7 Å) reflecting its more open nature. We note that these predictions are very similar to results obtained for the Σ5 MgO(310) tilt GB where models have been confirmed by high-resolution scanning transmission electron microscopy on bicrystals.[39]

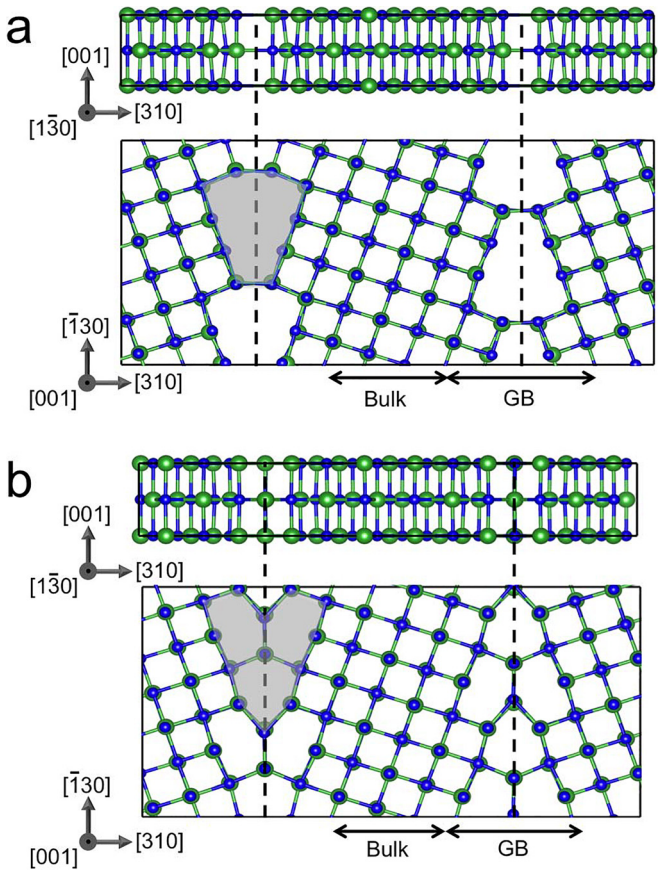

FIG. 1. The predicted stable structures of the Σ5 TiN(310)[001] grain boundary. (a) Grain boundary a is the most stable structure ($\gamma_a = 1.74$ J m^{-2}). (b) Grain boundary b is the second most stable structure ($\gamma_b = 1.78$ J m^{-2}). The green and blue spheres represent the titanium and nitrogen ions, respectively, and the dashed lines highlight the two grain boundary planes. The gray shaded areas indicate the regions inside the structural units which are prospective sites for oxygen incorporation.

The relative stability of the two GB structures can be quantified by the GB formation energy

$$\gamma = \frac{E_{GB} - NE_c}{2A},$$

where E_{GB} is the total energy of the fully optimized GB supercell, N is the number of TiN formula units in the GB supercell, E_c is the cohesive energy of bulk TiN, and A is the cross sectional area of the GB supercell. Despite the large difference in excess volume, we find the formation energies of the GBs are very similar ($\gamma_a = 1.74$ J m^{-2} and $\gamma_b = 1.78$ J m^{-2}). Detailed analysis of the atomic structure provides some insights into the origin of this effect. It is clear from the examination of Fig. 1 that although the structural unit in GB b is more compact just as many ions experience significant distortion from their bulk-like octahedral bonding configuration. In both GBs, the same number of Ti and N ions have their coordination number reduced to five and typical bond strains are of the order 1%–3%. Therefore, despite the difference in excess volume, the formation energy is similar because both GBs involve the creation of a very similar number of broken and strained bonds. The very close stability of these two possible structures suggests both may appear in real materials. In the discussion above, we have focused on total energies however, at finite pressure one should consider enthalpy in the place of the total energies above. Under atmospheric pressure, the enthalpy differs from the total energy of the GBs by the order of 10^{-4} J m^{-2}, insufficient to affect the relative stability. However, pressures in the MPa range would be sufficient to promote GB b to being the most stable as a result of its smaller excess volume and similar effects have been discussed previously for the structurally similar material MgO.[45]

B. Grain boundary electronic structure

With the GB structures determined, we turn to analyze the associated electronic properties (Fig. 2). For each GB, we calculate the electronic density of states (DOS) projected onto atoms in bulk and GB regions in the supercell (as highlighted in Fig. 1). As expected, the bulk DOS for both GB supercells is very similar and consistent with previous theoretical calculations.[26] Electronic states near the Fermi level have primarily a Ti 3d character, while states deeper within the valance band also have N 2p ($E - E_F < -2.5$ eV) and Ti 4s ($E - E_F < -6.0$ eV) contributions. For both GB structures, there is very little difference between the bulk and GB projected DOS near the Fermi energy. Only for deeper valance band states (in the range −5.5 to −3.0 eV) is a small upwards shift of about 0.4 eV for the GB electronic states apparent. We also find that the N 2s bands near to −15.5 eV exhibit an upward shift of about 0.6 eV at the GBs. Previous X-ray photoelectron spectroscopy studies of TiN found an asymmetrically shaped N 2s band centered around 16.5 eV consistent with our calculated DOS for the bulk.[18] Our prediction of a 0.6 eV upward shift in this band induced by GBs should be clearly distinguishable experimentally and

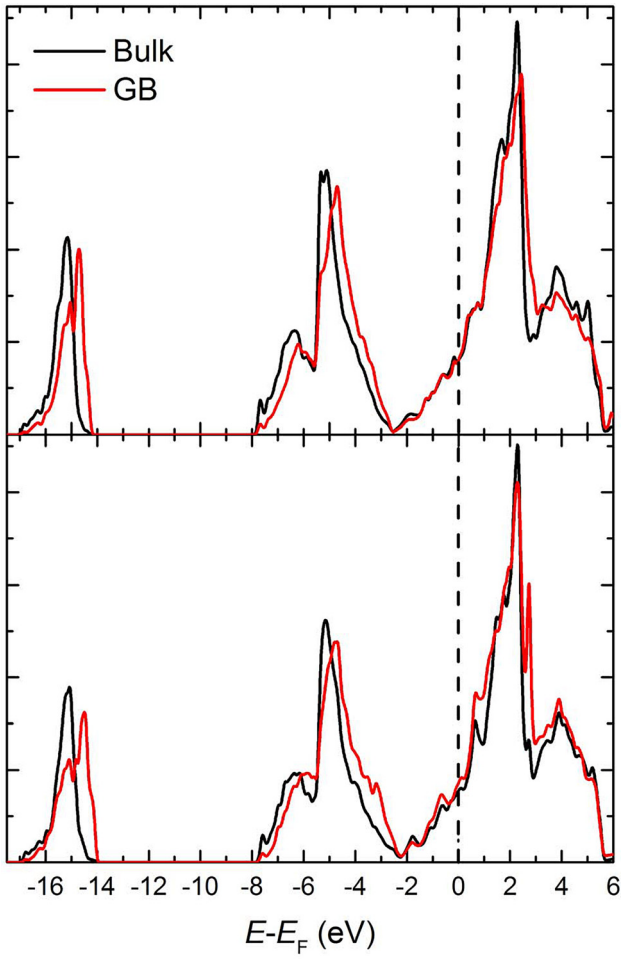

FIG. 2. Electronic density of states calculated for the Σ5 TiN(310)[001] grain boundaries (GB): GB a (upper panel) and GB b (lower panel). The projected density of states in the vicinity of the grain boundary (Fig. 1 shows the regions used for projections) and in the bulk of the grains (i.e., all ions are not in the grain boundary regions) is shown.

could be systematically studied on polycrystalline samples with different average grain size. Analysis of the average on-site electrostatic potential throughout the GB supercells provides an explanation for the upward shift of electronic states. We find that the electrostatic potential on sites within ±3 Å of the GB are shifted upwards by about 0.5 V which is consistent with the shifts seen in the DOS. We note that the local perturbation in both the structure and electrostatic potential at GBs is likely to induce increased electron scattering at the Fermi energy, thereby reducing conductivity, even though the DOS at the Fermi energy is barely modified.

C. Oxygen incorporation and diffusion in TiN

First, we address the incorporation of oxygen in the bulk TiN crystal. We consider incorporation of oxygen at the interstitial site (I) and since TiN is often N deficient[46] also at the N substitutional site (O_N). The incorporation energy with respect to an isolated oxygen molecule is calculated as

$$E_{\text{inc}} = E_{\text{ox}} - E_{\text{ideal}} - E_{O_2}/2,$$

where E_{ideal} is the total energy of the ideal supercell without oxygen, E_{ox} is the total energy of the ideal supercell with an additional oxygen atom, and E_{O_2} is the total energy of an isolated oxygen molecule (in the triplet state). Molecular oxygen represents a convenient and physically meaningful reference for the oxygen chemical potential. However, since PBE predicts a slight overbinding of the oxygen molecule, an *a posteriori* correction must be employed if absolute calibration of the chemical potential reference is required (e.g., see Ref. 47 and references within). However, we note that none of the conclusions in the present work rely upon an absolute calibration of the chemical potential since only relative stabilities are discussed. In all cases discussed below, we find that oxygen atoms incorporate in a non-spin polarized magnetic configuration. The incorporation energy for the interstitial site is +1.59 eV indicating that it is unfavorable for an oxygen molecule to dissociate and incorporate interstitially. The oxygen atom coordinates tetrahedrally to Ti ions in the lattice. Neighboring Ti ions relax inwards towards the O ion reducing the O-Ti distance to 1.91 Å [Fig. 3(b)]. Bader analysis of the charge density indicates the oxygen acquires a charge of $-1.2e$ explaining the attraction of the slightly electropositive Ti (we note the Bader charge of O ions in rutile TiO_2 calculated using the same method is also $-1.2e$ corresponding to a formal oxidation state of −2). The neighboring N ions relax outwards increasing the O-N distance to 2.33 Å. The low stability of this configuration can be understood in terms of the limited free space available compared to the size of the oxygen atom. On the other hand, the incorporation energy at the N substitutional site is −3.54 eV [Fig. 3(c)]. The six neighboring Ti ions relax outwards slightly by 0.12 Å on O substitution. Bader analysis indicates that in this case, the oxygen acquires a charge of $-1.3e$.

We next consider the incorporation of oxygen into the Σ5 TiN(310)[001] GB (GB a and GB b). We insert an O atom at various positions inside the dislocation cores (shaded areas in Fig. 1). For each prospective position, full geometry optimization is performed and in this way the most stable configuration is identified. The most stable configurations for GB a and GB b are shown in Figs. 3(c) and 3(d). For GB a (hereafter O_a), the oxygen atom forms bonds with two undercoordinated Ti ions and sits in a position on one side of the GB symmetry plane. The incorporation energy for this configuration is −3.10 eV. We also investigated incorporation of oxygen in a molecular configuration by adding two O atoms to the GB. However, we find that the oxygen molecule is unstable to dissociation and the oxygen atoms prefer to be separated. Bader analysis provides an explanation for this effect as it shows each oxygen atom acquires a charge of $-1.1e$ which favors dissociation as O_2^{2-} is not a stable molecular species (except in high Madelung potentials in highly ionic materials). For GB b (hereafter O_b), the smaller volume of the dislocation core means the oxygen atom instead sits on the GB symmetry plane forming bonds with three undercoordinated Ti ions. The incorporation energy is correspondingly reduced to −1.33 eV. Again, we verified that incorporation of molecular oxygen is not favorable and Bader analysis indicates the O atom in the GB carries a charge of $-1.2e$. We also considered the interaction of N and Ti vacancy defects with the GB, however, found no

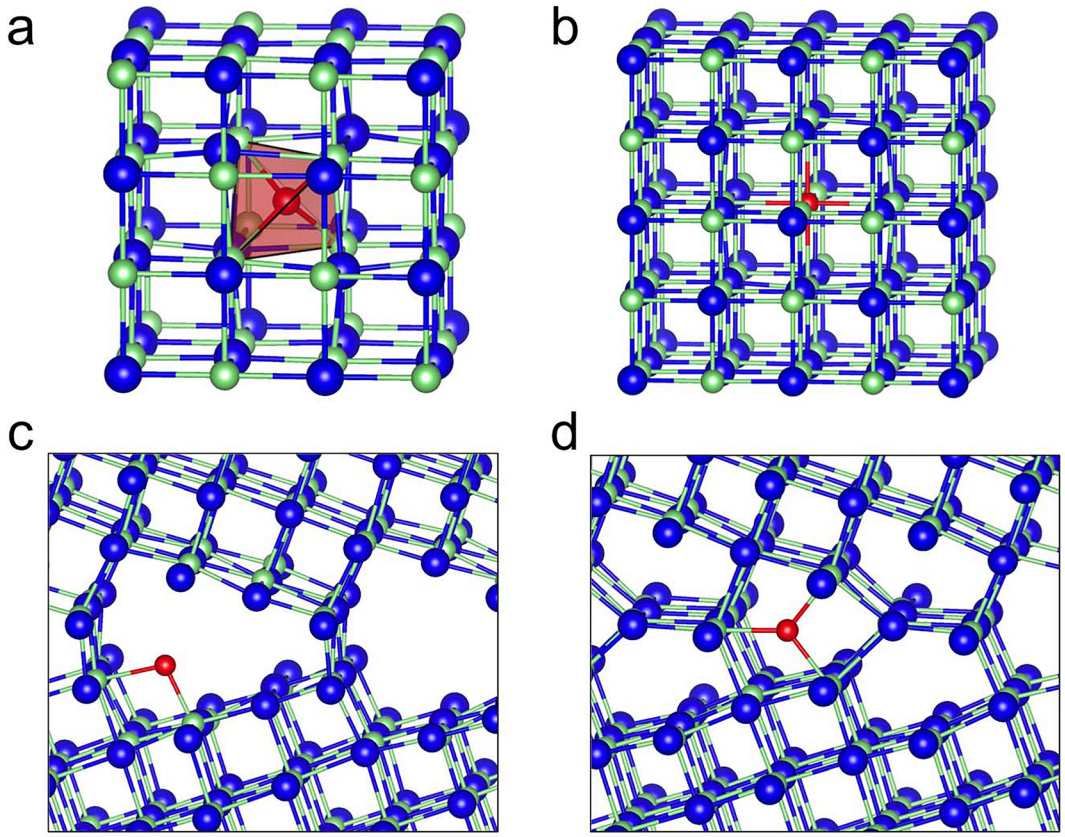

FIG. 3. Stable sites for incorporation of oxygen in TiN. (a) Interstitial site, (b) nitrogen substitutional site, (c) GB a, and (d) GB b. The green and blue spheres represent the titanium and nitrogen ions, respectively.

significant tendency for segregation consistent with recent results for a similar GB in TiN.[28]

Having identified stable incorporation sites for oxygen in TiN GBs, we now address the mechanism and kinetic barrier to diffusion. The climbing image NEB method is used to estimate the activation barrier to diffusion along the dislocation core (see Sec. III). Figure 4 shows the predicted pathways for oxygen diffusion in both GBs. The calculated barrier to oxygen diffusion between equivalent adsorption sites in GB a is 1.74 eV. The transition state involves the oxygen atom bonding to two Ti and two N atoms in a four-fold follow site. The barrier for GB b is 2.11 eV, slightly higher owing to the reduced free space available. The transition state involves the oxygen atom binding to four Ti and three N atoms. Both of these barriers are too high to expect significant mobility at room temperature.

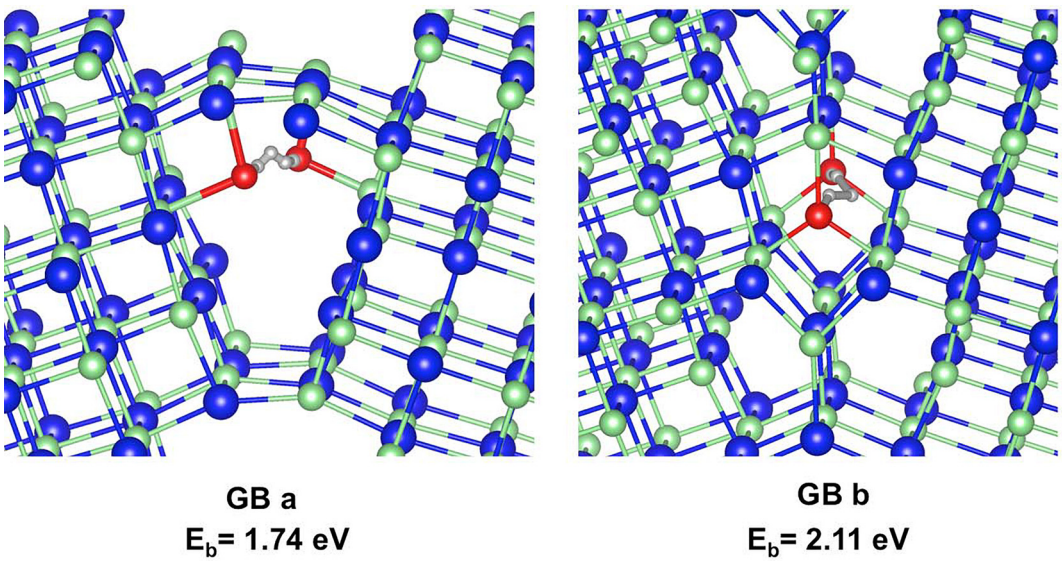

FIG. 4. Oxygen diffusion paths and barriers to diffusion for the Σ5 TiN(310)[001] grain boundaries GB a and GB b. The green, blue, and red spheres represent the titanium, nitrogen, and oxygen ions, respectively. The small grey spheres connected by lines depict the pathways for oxygen diffusion.

D. Oxygen exchange between *m*-HfO_2 and TiN

To address the thermodynamics of oxygen exchange between *m*-HfO_2 and TiN, we first perform calculations of the energy to extract oxygen from *m*-HfO_2. In particular, we consider extraction of oxygen from lattice sites (both three- and four-coordinated oxygen sites) and interstitial oxygen. While calculations of the formation energy of these defects have been performed previously, it is necessary to calculate them again using a consistent computational method into order to accurately determine exchange energies.[12] The energy to extract a neutral oxygen atom (i.e., the oxygen vacancy formation energy) is calculated as

$$E_{ex} = E_{aft} - E_{bef} + E_{O_2}/2,$$

where E_{bef} and E_{aft} are the total energies of the system before and after oxygen extraction. We calculated an extraction energy of 6.47 eV and 6.33 eV for the three- and four-coordinated lattice oxygen in good agreement with previous calculations[12] [3C and 4C in Fig. 5(a)]. We also consider the extraction of oxygen from an interstitial site [see I in Fig. 5(a)]. The extraction energy for the oxygen interstitial is −1.75 eV, again consistent with previous calculations. In other words, the oxygen interstitial in *m*-HfO_2 is thermodynamically unfavorable, but we note it may be generated in non-equilibrium processes in ReRAM device operation as discussed in the literature.[3,4,48,49]

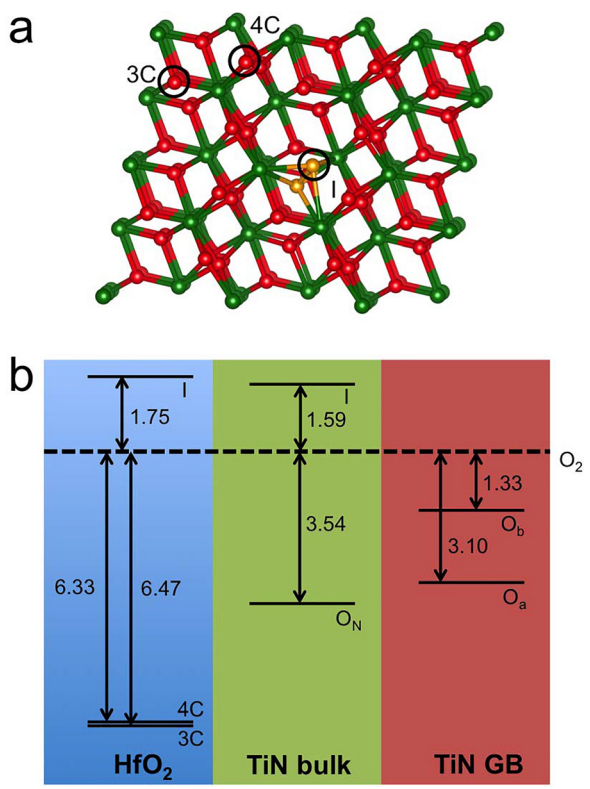

FIG. 5. (a) Three- (3C) and four-coordinated (4C) lattice oxygen and interstitial (I) oxygen sites in *m*-HfO_2. The green and red spheres represent the hafnium and oxygen ions, respectively. The neutral oxygen interstitial forms a dimer configuration with one of the lattice oxygen atoms (both atoms of the dimer are highlighted in orange in the figure). (b) An energy diagram summarizing the stability of the different oxygen sites in *m*-HfO_2, TiN bulk, and TiN grain boundaries relative to an O_2 molecule (all energies are shown in eV).

The extraction and incorporation energies that govern oxygen exchange between *m*-HfO_2 and TiN are shown schematically in Fig. 5. It can be seen that transfer of oxygen from lattice sites in *m*-HfO_2 to nitrogen vacancies in TiN costs at least 2.8 eV, while transfer to GB sites costs at least 3.2 eV. On the other hand, interstitial oxygen in *m*-HfO_2 will readily incorporate into TiN (nitrogen vacancies or GBs) gaining upwards of 3 eV depending on the stability of the incorporation site. For more reducible oxides, oxygen transfer into GBs may be more favorable (see below for a more detailed discussion).

V. DISCUSSION

Direct experimental information on the electronic properties of GBs in TiN is scarce. As discussed in Sec. II, there is evidence from transport measurements and spectroscopic ellipsometry that GBs limit the electron mean free path in polycrystalline TiN due to increased scattering rather than a reduction of the density of states at the Fermi energy.[7,8] This idea is consistent with the results presented in this paper - namely, that although the local DOS at the Fermi level is not significantly modified at GBs, the structure and electrostatic potential are, which gives rise to increased electron scattering and reduced conductivity. Our results suggest the effect of GBs on electronic properties could be more easily quantified by examining the N 2*s* band which is predicted to be upshifted by about 0.6 eV at the GB. For example, it should be straightforward to characterize the N 2*s* band (e.g., using X-ray photoelectron spectroscopy) for TiN samples of different grain size in order to extract the contribution from GBs, thereby providing an experimental characterization of the local electrostatic perturbation.

Our calculations show that incorporation of oxygen into bulk TiN is only favorable at nitrogen vacancy sites. On the other hand, for both of the TiN GBs considered, oxygen incorporates gaining up to 3.1 eV per oxygen atom with respect to molecular oxygen. The predicted preferential oxidation of GBs in TiN is consistent with previous experimental studies.[9] The oxygen molecule is shown to dissociate into oxygen atoms at the GB which coordinate with Ti atoms and acquire a negative charge of approximately $-1e$.

To assess the possibility of oxygen transfer between *m*-HfO_2 and an adjacent TiN layer, we computed corresponding oxygen removal and incorporation energies for a range of possible sites. These calculations show that it costs at least 3.2 eV to transfer a lattice oxygen from HfO_2 into a TiN GB. Although oxygen ions may be less strongly bound near the TiN interface (due to undercoordination and strain), this very high energy suggests such a process is unlikely. Therefore, TiN should represent very a benign electrode for MOSFET applications. However, if interstitial oxygen is present in HfO_2 (which could be generated by large electric fields in a ReRAM device, for example Refs. 3, 15, and 16), it may readily incorporate into TiN GBs.

Diffusion of oxygen along the dislocation cores at GBs is predicted to be a slow process with activation energies upwards of 1.7 eV. Taking this lower limit and assuming a simple Arrhenius dependence of the transition rate (and an

attempt frequency of the order 10^{12} Hz), we estimate temperatures of the order 700 °C would be need to drive appreciable diffusion (i.e., transition rates faster than 10^3 Hz). Therefore, at ambient temperatures, once oxygen is incorporated into TiN GBs, it acts as an obstacle to incorporation and diffusion of further oxygen (or other species). This finding is consistent with the "stuffed barrier model" proposed to explain the good barrier characteristics of air exposed polycrystalline TiN with applications in microelectronics.[11,24]

If one considers interfaces between TiN and other more reducible oxides, the situation could be very different. For example, previous calculations have put the oxygen vacancy formation energy for GeO_2 below 4 eV (Ref. 50), in which case transfer of oxygen from GeO_2 to TiN GBs would cost less than 1 eV. One should also note that if the oxide layer is also polycrystalline, oxygen vacancy formation energies may be reduced further still[39,51] and spontaneous local reduction of the oxide near TiN GBs may become very likely.

The first principles calculations presented above elucidate the structure, electronic, and defect segregation properties of the Σ5 TiN(310)[001] tilt GB. We have focused on one particular GB type as a model system (albeit with two distinct stable structures) due to the computationally demanding nature of the calculations. In reality, real materials will contain a wider range of GBs corresponding to different crystal orientations. However, we note GBs often exhibit qualitatively similar features, namely undercoordination, local strain, and variation in the GB excess volume. Therefore, while the present results address a specific GB as an example, we expect the results obtained to be a reasonable guide for more general GBs.

The calculations in the article have employed the PBE exchange-correlation functional. It is well known that the PBE functional underestimates the band gaps of wide gap materials like HfO_2. However, important structural properties and oxygen vacancy defect formation energies are described well. The depth of the core and semi-core states (e.g., N 2*s*) in TiN appear slightly underestimated with respect to the experiment.[18] However, the relative differences (with respect to the bulk crystal) of the structural and electronic properties induced by GBs are however expected to be more reliable. Hybrid exchange-correlation functionals can give a better description of wide gap oxides, but often provide a poorer description of metallic materials like TiN. Therefore, on balance the PBE functional represents a better compromise for this study.

VI. CONCLUSIONS

In summary, we have performed a detailed theoretical investigation of the structure, electronic properties, and oxygen incorporation/diffusion characteristics of the Σ5 TiN(310)[001] tilt GB using first principles methods. We identify two inequivalent structures for the (310) tilt GB (with very similar stability) corresponding to different rigid body translations of one crystal with respect to the other. Analysis of the electronic structure reveals that these GBs do not significantly modify electronic states near the Fermi energy but do induce an upwards shift of up to 0.6 eV in a number of deeper occupied bands. The homogeneity of the density of states at the Fermi energy is an advantage for applications of TiN as a gate metal and is in contrast to polycrystalline silicon, where GBs contribute to significant threshold variability in *n*-type transistors.[37] We also show that oxygen is preferentially incorporated into the TiN GB but must overcome relatively high activation energies for further diffusion. This prediction is consistent with the "stuffed barrier model" proposed to explain the good barrier characteristics of TiN.[11,24] Furthermore, we have shown while the oxidizing power of TiN GBs is not sufficient to reduce HfO_2 (a prototypical gate dielectric material), they can act as a scavenger for interstitial oxygen. This may be important in ReRAM devices where large electric fields and Joule heating can drive interstitial generation.[3,15,16] Altogether, these results provide much needed atomistic insights into the properties of a model GB in TiN and suggest a number of directions for future investigation.

ACKNOWLEDGMENTS

K.P.M. acknowledges support from the EPSRC (EP/K003151, EP/P006051/1 and EP/P023843/1) and COST Action CM1104. This work made use of the facilities of Archer, the UK's national high-performance computing service, via our membership in the UK HPC Materials Chemistry Consortium, which is funded by the EPSRC (EP/L000202). K.P.M. also thanks Alex Shluger for the helpful discussions.

APPENDIX: DATA ACCESS STATEMENT

All data created during this research are available by request from the University of York Research database http://dx.doi.org/10.15124/eb65549b-d598-4ef5-9b0b-be3b48340fe9.

[1]J. Robertson and R. M. Wallace, Mater. Sci. Eng., R **88**, 1 (2015).
[2]R. Waser and M. Aono, Nat. Mater. **6**, 833 (2007).
[3]L. Goux, P. Czarnecki, Y. Y. Chen, L. Pantisano, X. P. Wang, R. Degraeve, B. Govoreanu, M. Jurczak, D. J. Wouters, and L. Altimime, Appl. Phys. Lett. **97**, 243509 (2010).
[4]G. Bersuker, D. C. Gilmer, D. Veksler, P. Kirsch, L. Vandelli, A. Padovani, L. Larcher, K. P. McKenna, A. Shluger, V. Iglesias, M. Porti, and M. Nafria, J. Appl. Phys. **110**, 124518 (2011).
[5]F. Pan, S. Gao, C. Chen, C. Song, and F. Zeng, Mater. Sci. Eng., R **83**, 1 (2014).
[6]A. E. Kaloyeros and E. Eisenbraun, Annu. Rev. Mater. Sci. **30**, 363 (2000).
[7]P. Patsalas and S. Logothetidis, J. Appl. Phys. **90**, 4725 (2001).
[8]H. V. Bui, A. Kovalgin, and R. Wolters, Appl. Surf. Sci. **269**, 45 (2013).
[9]N. C. Saha and H. G. Tompkins, J. Appl. Phys. **72**, 3072 (1992).
[10]M. Mändl, H. Hoffmann, and P. Kücher, J. Appl. Phys. **68**, 2127 (1990).
[11]H. G. Tompkins, J. Appl. Phys. **70**, 3876 (1991).
[12]A. S. Foster, F. Lopez Gejo, A. L. Shluger, and R. M. Nieminen, Phys. Rev. B **65**, 174117 (2002).
[13]M. Jo, H. Park, M. Chang, H.-S. Jung, J.-H. Lee, and H. Hwang, Microelectron. Eng. **84**, 1934 (2007).
[14]E. Cartier and A. Kerber, in *2009 IEEE International Reliability Physics Symposium* (2009), pp. 486–492.
[15]S. R. Bradley, K. P. McKenna, and A. L. Shluger, Microelectron. Eng. **109**, 346 (2013).
[16]W. Kim, S. Menzel, D. J. Wouters, Y. Guo, J. Robertson, B. Roesgen, R. Waser, and V. Rana, Nanoscale **8**, 17774 (2016).
[17]B. Subramanian, C. Muraleedharan, R. Ananthakumar, and M. Jayachandran, Surf. Coat. Technol. **205**, 5014 (2011).

[18]M. Delfino, J. A. Fair, and D. Hodul, J. Appl. Phys. **71**, 6079 (1992).
[19]N. Schönberg, Acta Chem. Scand. **8**, 213 (1954).
[20]N. Mosavati, V. R. Chitturi, S. O. Salley, and K. S. Ng, J. Power Sources **321**, 87 (2016).
[21]G. V. Naik, J. L. Schroeder, X. Ni, A. V. Kildishev, T. D. Sands, and A. Boltasseva, Opt. Mater. Express **2**, 478 (2012).
[22]S. Li, C. Sun, and H. Park, Thin Solid Films **504**, 108 (2006).
[23]J. J. Bean, M. Saito, S. Fukami, H. Sato, S. Ikeda, H. Ohno, Y. Ikuhara, and K. P. McKenna, Sci. Rep. **7**, 45594 (2017).
[24]W. Sinke, G. P. A. Frijlink, and F. W. Saris, Appl. Phys. Lett. **47**, 471 (1985).
[25]R. Bès, Y. Pipon, N. Millard-Pinard, S. Gavarini, and M. Freyss, Phys. Rev. B **87**, 024104 (2013).
[26]M. Marlo and V. Milman, Phys. Rev. B **62**, 2899 (2000).
[27]S. Yadav, R. Ramprasad, A. Misra, and X.-Y. Liu, Acta Mater. **74**, 268 (2014).
[28]M. N. Popov, A. S. Bochkarev, V. I. Razumovskiy, P. Puschnig, and J. Spitaler, Acta Mater. **144**, 496 (2018).
[29]G. Kresse and J. Furthmüller, Phys. Rev. B **54**, 11169 (1996).
[30]G. Kresse and J. Furthmüller, Comput. Mater. Sci. **6**, 15 (1996).
[31]P. E. Blöchl, Phys. Rev. B **50**, 17953 (1994).
[32]G. Kresse and D. Joubert, Phys. Rev. B **59**, 1758 (1999).
[33]J. P. Perdew, K. Burke, and M. Ernzerhof, Phys. Rev. Lett. **77**, 3865 (1996).
[34]J. Adam and M. D. Rogers, Acta Crrystallogr. **12**, 951 (1959).
[35]A. Kornilov, I. Ushakova, E. Huber, and C. Holley, J. Chem. Thermodyn. **7**, 21 (1975).
[36]M. W. Chase, Jr., J. Phys. Chem. Ref. Data, Monogr. **9**, 1 (1998).
[37]A. Asenov, A. Cathignol, B. Cheng, K. P. McKenna, A. R. Brown, A. L. Shluger, D. Chanemougame, K. Rochereau, and G. Ghibaudo, IEEE Electron Device Lett. **29**, 913 (2008).
[38]K. P. McKenna and A. L. Shluger, Nat. Mater. **7**, 859 (2008).
[39]K. P. McKenna and A. Shluger, Phys. Rev. B **79**, 224116 (2009).
[40]K. McKenna and A. Shluger, Appl. Phys. Lett. **95**, 222111 (2009).
[41]S. K. Wallace and K. P. McKenna, Adv. Mater. Interfaces **1**, 1400078 (2014).
[42]J. J. Bean and K. P. McKenna, Acta Mater. **110**, 246 (2016).
[43]G. Henkelman, A. Arnaldsson, and H. Jónsson, Comput. Mater. Sci. **36**, 354 (2006).
[44]D. Sheppard, R. Terrell, and G. Henkelman, J. Chem. Phys. **128**, 134106 (2008).
[45]X.-Y. Sun, V. Taupin, P. Cordier, C. Fressengeas, and B. B. Karki, J. Mater. Res. **31**, 3108 (2016).
[46]H. Höchst, R. D. Bringans, P. Steiner, and T. Wolf, Phys. Rev. B **25**, 7183 (1982).
[47]Y. A. Mastrikov, E. Heifets, E. Kotomin, and J. Maier, Surf. Sci. **603**, 326 (2009).
[48]J. Yang, F. Miao, M. Pickett, D. A. A. Ohlberg, D. R. Stewart, C. N. Lau, and R. S. Williams, Nanotechnology **20**, 215201 (2009).
[49]S. Abdelouahed and K. P. McKenna, J. Appl. Phys. **118**, 134103 (2015).
[50]Y. Guo and J. Robertson, Appl. Phys. Lett. **105**, 223516 (2014).
[51]K. P. McKenna, A. Shluger, V. Iglesias, M. Porti, M. Nafría, M. Lanza, and G. Bersuker, Microelectron. Eng. **88**, 1272 (2011).